Microstructure and secondary phases in coevaporated $CuInS_2$ films: Dependence on growth temperature and chemical composition

J. Álvarez-García, A. Pérez-Rodríguez,[a] A. Romano-Rodríguez, and J. R. Morante
Lab. Enginyeria i Materials Electrònics (EME), Unitat Associada Centre Nacional de Microelectronica (CNM-CSIC), Departament d'Electrònica, Universitat de Barcelona, Martí i Franquès 1, 08028 Barcelona, Spain

L. Calvo-Barrio
Serveis Científico-Tècnics, Universitat de Barcelona, Lluís Solé i Sabarís 1-3, 08028 Barcelona, Spain

R. Scheer and R. Klenk
Hahn-Meitner Institute, Glienicker Strasse 100, D-14109 Berlin, Germany

(Received 30 March 2000; accepted 2 October 2000)

The microstructure of $CuInS_2$ (CIS_2) polycrystalline films deposited onto Mo-coated glass has been analyzed by Raman scattering, Auger electron spectroscopy (AES), transmission electron microscopy, and x-ray diffraction techniques. Samples were obtained by a coevaporation procedure that allows different Cu-to-In composition ratios (from Cu-rich to Cu-poor films). Films were grown at different temperatures between 370 and 520 °C. The combination of micro-Raman and AES techniques onto Ar^+-sputtered samples has allowed us to identify the main secondary phases from Cu-poor films such as $CuIn_5S_8$ (at the central region of the layer) and MoS_2 (at the CIS_2/Mo interface). For Cu-rich films, secondary phases are CuS at the surface of as-grown layers and MoS_2 at the CIS_2/Mo interface. The lower intensity of the MoS_2 modes from the Raman spectra measured at these samples suggests excess Cu to inhibit MoS_2 interface formation. Decreasing the temperature of deposition to 420 °C leads to an inhibition in observing these secondary phases. This inhibition is also accompanied by a significant broadening and blueshift of the main A_1 Raman mode from CIS_2, as well as by an increase in the contribution of an additional mode at about 305 cm^{-1}. The experimental data suggest that these effects are related to a decrease in structural quality of the CIS_2 films obtained under low-temperature deposition conditions, which are likely connected to the inhibition in the measured spectra of secondary-phase vibrational modes. © *2001 American Vacuum Society.* [DOI: 10.1116/1.1329123]

I. INTRODUCTION

$CuInS_2$ (CIS_2) is a chalcogenide semiconductor that has potential for high-efficiency solar cell devices. It is characterized by a band-gap value (1.5 eV) that is well adapted to terrestrial as well as space applications. Recently, a CIS_2-based solar cell with a total area efficiency of 11.4% was reported.[1] However, this is still beyond the efficiencies currently obtained in $CuInSe_2$-based devices. Further improvement in the efficiency of the cells requires a better understanding of the microstructure of the polycrystalline CIS_2 layers and the microstructure's dependence on the technological processes.

One of the best-suited techniques for structurally assessing these layers is Raman scattering.[2] The Raman spectrum from $CuInS_2$ is characterized by the presence of a dominant A_1 mode, at about 290 cm^{-1}, which corresponds to the vibration of *S* anions in the $X-Y$ crystallographic directions of the tetragonal cell.[3] The position and width of this peak are very sensitive to structural features, such as disorder of the cation sublattice, stress, and structural defects. Also, films obtained under conditions leading to poor structural quality show an additional mode at about 305 cm^{-1}.[3,4] The origin of this mode is still not clear. Its relative intensity in relation to that of the A_1 mode correlates with the increase in the shift and broadening of the A_1 peak. The comparison of these features with x-ray diffraction (XRD) and transmission electron microscopy (TEM) data show them to be clearly related to the overall structural quality of the films, which supports the assumption of a structural-related origin of the mode.

This work reports on the microstructural characterization of CIS_2 layers obtained by a coevaporation process at different temperatures and with different chemical compositions. For this, Raman scattering data have been correlated with the analysis of the films by Auger electron spectroscopy (AES), XRD, and TEM techniques. The combination of a Raman microprobe with a scanning AES nanoprobe system has allowed us to develop a detailed study of the films, in terms of structural quality, composition, and presence of secondary phases.

II. EXPERIMENTAL DETAILS

Polycrystalline films of $CuInS_2$ have been grown on Mo-coated soda-lime glass substrates by coevaporation of Cu, In, and S. Due to the separation of the indium and copper sources, a layer with a lateral gradient composition is obtained, being Cu rich for about half of the layer and Cu poor

[a]Electronic mail: perez-ro@el.ub.es

 0734-2101/2001/19(1)/232/8/$18.00 ©2001 American Vacuum Society

for the other half. Four different samples have been grown at different temperatures (520, 470, 420, and 370 °C) to study the effect of this parameter.

At the Cu-rich region of the samples, segregation of Cu excess occurs at the surface of the layers in the form of CuS. This is removed by chemical etching in a 10% KCN solution. Etching of the whole CuS layer is observed by the disappearance of all CuS peaks from both surface Raman and XRD spectra. Films have an average thickness of 2.5 μm, and the dimensions of the samples are 5 cm×0.8 cm.

Micro-Raman scattering measurements were performed at room temperature with a Jobin–Yvon T64000 spectrometer coupled with an Olympus metallographic microscope, using the green line of an Ar^+ laser (λ=514.5 nm) as excitation light. For the objective used (X100, NA=0.95), the spot size on the sample is slightly submicronic. Spectra were obtained in a backscattering configuration, collecting light from all possible polarizations. In these conditions, the depth investigated by the Raman microprobe is determined by the optical absorption of light in $CuInS_2$, with the absorption length being about 100 nm. To avoid thermal effects in the spectra—which are especially conspicuous for these measurements where a relatively high power density can be achieved at the scattering volume spectra—the excitation power of light on the sample has been kept below 1 mW. This corresponds to a power surface density below 0.29×10^6 W/cm^2. All the measured spectra have been compared with those obtained at the same conditions on single-crystal stoichiometric $CuInS_2$ (reference sample).

Previous Raman scattering measurements performed at the surface of the samples show a dominant contribution of the 305 cm^{-1} mode at the Cu-poor region for all the samples.[3] This is also accompanied by a significant blueshift and broadening of the A_1 mode. For the Cu-rich side, the spectra show a higher dependence on the temperature of deposition: For the samples deposited at the highest temperatures (520,470 °C), the spectra are similar to that from the reference $CuInS_2$ sample. However, for the samples deposited at the lowest temperatures (420,370 °C), the spectra show the presence of the additional 305 cm^{-1} mode, together with the corresponding blueshift and broadening of the A_1 mode. These data indicate the existence of two distinct behaviors, corresponding to high-temperature (520,470 °C) and low-temperature (420,370 °C) deposition conditions. Accordingly, the detailed analysis of the samples has focused mainly in the samples deposited at 520 and 370 °C. In the following discussion, these are referred to as the high-temperature and low-temperature cases, respectively.

For Auger measurements, a PHI 670 Scanning Auger Nanoprobe System model has been used. The electron-beam energy was 10 keV, with a current of 10 nA. The beam diameter was below 100 nm, and the scanned area in the samples was about 10 μm×15 μm. To quantify the chemical composition, AES measurements were performed on the single-crystal reference $CuInS_2$, and these data were used as standards to define the corrective factors. For the ion sputtering of the sample, an Ar^+ ion gun was used, with nominal values of energy and current of 2 keV and 50 μA, respectively. In-depth Raman measurements were made by focusing the light spot in this region, after equivalent sputter steps of 15 min. These in-depth measurements were performed at equivalent points from both Cu-rich and Cu-poor regions, located at 0.5 cm from the respective edges. Raman scattering measurements performed on the sputtered surface from a single-crystal $CuInS_2$ sample have revealed the absence of significant damage effects related to the sputter process.

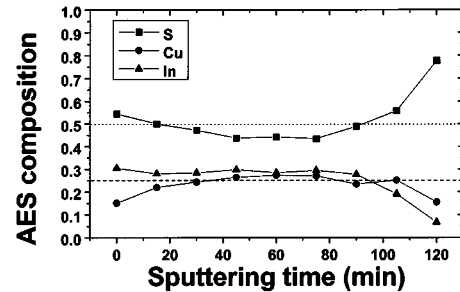

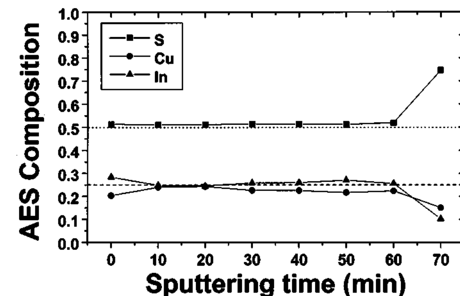

FIG. 1. AES depth composition profiles from the Cu-poor samples deposited at (a) 520 and (b) 370 °C. Stoichiometric $CuInS_2$ composition is indicated by dotted lines.

These data were correlated with the analysis of selected layers by XRD. Standard $\theta/2\theta$ XRD spectra were measured with a Siemens D-500 spectrometer in Bragg–Bentano configuration. Finally, the cross-section TEM analysis of the layers was performed in a Philips CM30 microscope operated at 300 keV and in a Phillips CM200 SuperTwin microscope, equipped with a field emission gun, operated at 200 keV, by observing specimens prepared according to the procedure described in Ref. 5.

III. RESULTS

A. In-depth Raman AES: Cu poor

Figure 1 shows the AES chemical composition profiles from the samples deposited at the highest (a) and lowest (b) temperatures. In both cases, a surface Cu-depleted region is observed, extending down to about 10%–20% of the layer. Below this region, the In content tends to be higher than the Cu, with the [In]/{[In]+[Cu]} ratio being in the range of 0.50–0.55. The integral [In]/{[In]+[Cu]} composition ratio in the bulk of the samples is 0.54 (high-temperature case) and 0.53 (low-temperature case). The deviations observed

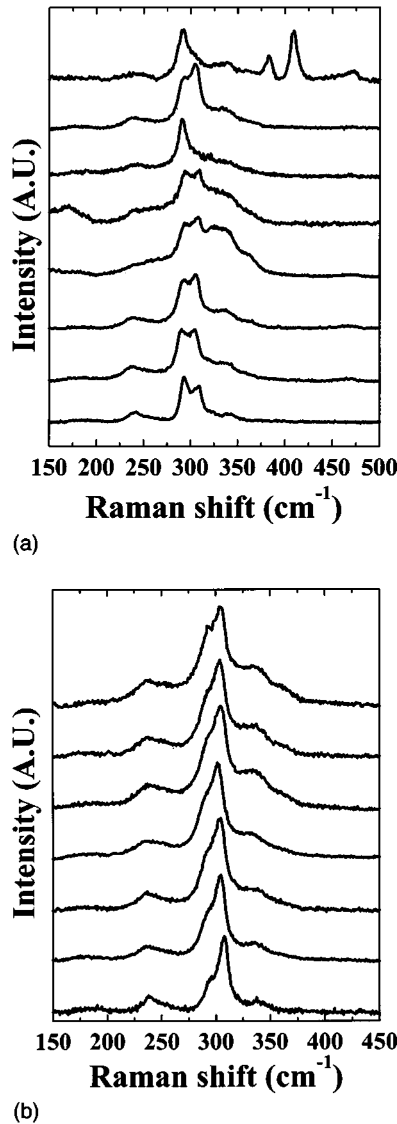

FIG. 2. Raman spectra from sputtered Cu-poor samples deposited at (a) 520 and (b) 370 °C. The spectra are normalized to the intensity of the dominant mode. The spectrum at the bottom corresponds to the surface of the layers, and spectra measured after consecutive sputter steps are shifted vertically.

for the measurements performed at the deepest regions (close to the CIS_2/Mo interface) are related to the high uncertainty in the measurements. This uncertainty is due to overlapping between the Mo and S signals, which explains the sharp increase in the intensity of the S signal.

The whole series of Raman spectra measured after each sputter step in both samples are shown in Figs. 2(a) and 2(b), respectively. All these spectra are characterized by the additional mode at about 305 cm^{-1}, which in some cases becomes even higher than the CIS_2 A_1 mode. Also, the film deposited at the highest temperature shows the presence of additional modes at higher frequencies, which appear mainly at the central region of the layer. These modes can be fitted with three Lorentzians, centered at about 325, 340, and 360 cm^{-1}, respectively. These positions correspond to those reported for the three strongest vibrational modes of $CuIn_5S_8$,[6] which points out the presence of this secondary phase in the

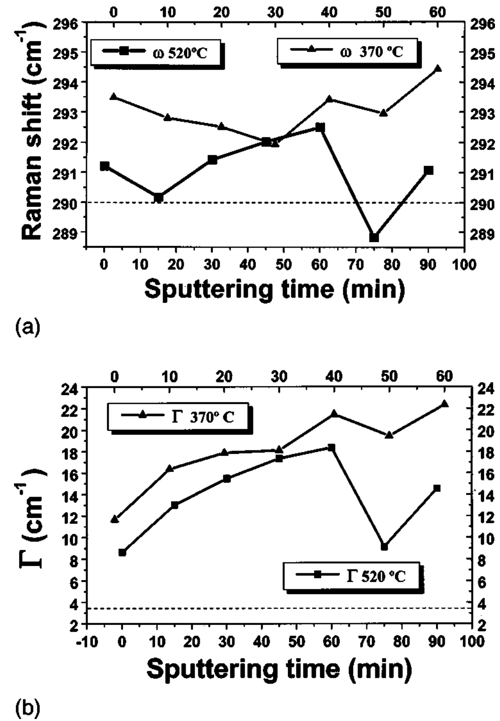

FIG. 3. Position (a) and FWHM (b) of the A_1 Raman peak vs sputtering time from the sputtered Cu-poor samples deposited at 520 and 370 °C. Dotted lines indicate the spectral features of the A_1 mode as measured from the reference sample.

central region of the Cu-poor layer. This has also been corroborated by XRD measurements, which show the presence of randomly oriented $CuIn_5S_8$ crystals in the layer. The spectrum measured at the deepest position also shows additional peaks at 382 and 408 cm^{-1}. These peaks will be discussed later.

Lowering of the temperature of deposition leads to a significant decrease in the spectral contribution from the $CuIn_5S_8$ secondary phase [Fig. 2(b)]. This phase appears mainly at the lower half of the layer and tends to increase with depth. Also, the spectra measured from this sample are characterized by a higher intensity of the 305 cm^{-1} mode, which is the dominant one. Dominance of the 305 cm^{-1} mode is also accompanied by an increase in both blueshift and broadening of the A_1 mode from this layer in relation to that from the layer deposited at high temperature. This is shown in Figs. 3(a) and 3(b), where the Raman shift and full width at half maximum (FWHM) of the A_1 mode are plotted versus sputtering time for both samples. This behavior indicates a clear decline in structural quality of the layer deposited at low temperature.

B. In-depth Raman AES: Cu rich

In comparison with Cu-poor films, the Cu-rich ones are characterized by a much stronger dependence of chemical composition on processing temperature, as seen in Figs. 4(a) and 4(b). For the sample deposited at 520 °C [Fig. 4(a)], the in-depth AES profile is similar to that from the corresponding Cu-poor sample [Fig. 2(a)]: At the surface, there is a thin

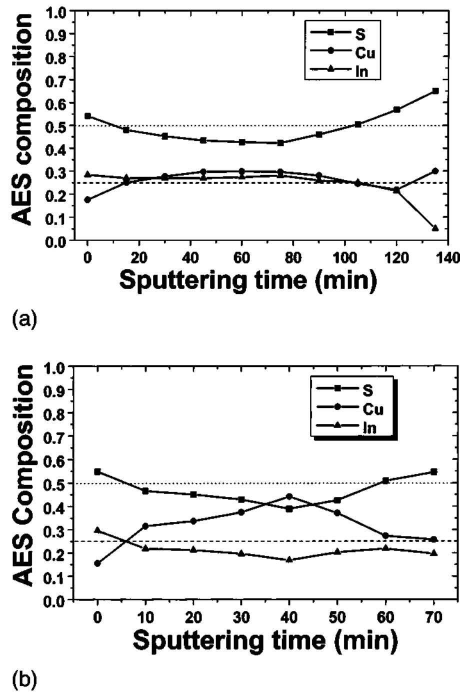

FIG. 4. AES depth composition profiles from the Cu-rich etched samples deposited at (a) 520 and (b) 370 °C. Stoichiometric $CuInS_2$ composition is indicated by dotted lines.

Cu-depleted region, and below this region the In and Cu contents in the layer are very similar, the [In]/{[Cu]+[In]} content ratio being close to stoichiometry (in the range of 0.47–0.50). The integral [In]/{[In]+[Cu]} composition ratio in the bulk of this sample is 0.49. Decreasing the temperature of deposition to 370 °C leads to drastic changes [Fig. 4(b)]: In this case, the Cu cation content is higher than the In cation content at the whole layer, except for the first point (at the surface), due to the surface Cu-depleted region. This leads to a significant deviation from stoichiometry of the integral composition ratio of the layer ([In]/{[In]+[Cu]}=0.375).

The corresponding Raman spectra are shown in Figs. 5(a) and 5(b). For the sample deposited at high temperature [Fig. 5(a)], the spectra measured at different depths are very similar, always being characterized by a dominant A_1 contribution, and no significant contribution from any secondary phase is observed. Although some of the spectra show a certain contribution at the 300–360 cm^{-1} region, this is likely related to sputter-induced damage. Similar sputter-induced effects have been observed from the stoichiometric single-crystal $CuInS_2$ reference sample.

For the film deposited at low temperature [Fig. 5(b)], the most striking feature in the spectra is the presence of the 305 cm^{-1} mode, which is detected in the majority of the spectra in the layer. Also, we emphasize the absence of any contribution from CuS vibrational modes in the spectra, in spite of the high Cu content in the layer. The appearance of the 305 cm^{-1} mode is also accompanied by a significant increase in the broadening of the A_1 CIS_2 mode in relation to that from the high-temperature case [Fig. 6(b)]. The position of the mode is also affected, and the mode becomes blueshifted,

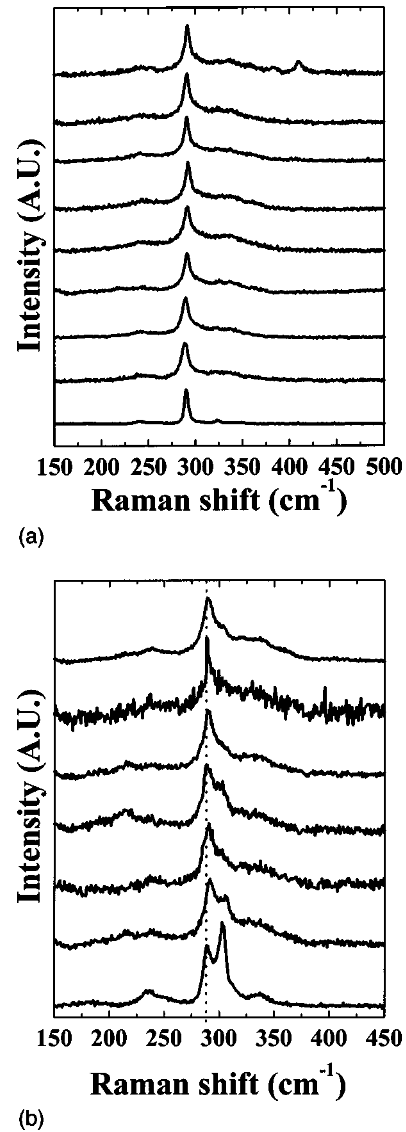

FIG. 5. Raman spectra from sputtered Cu-rich etched samples deposited at (a) 520 and (b) 370 °C. The spectra are normalized to the intensity of the dominant mode. The spectrum at the bottom corresponds to the surface of the layers, and spectra measured after consecutive sputter steps are shifted vertically. The high noise level in the spectrum in Fig. 6(b) close to the CIS_2/Mo interface is likely related to a bad focusing during the measurement.

whereas for the sample grown at high temperature, a redshift is observed [Fig. 6(a)], characteristic of layers deposited under Cu-excess conditions. This behavior agrees with that observed from the Cu-poor region of the samples and points out the existence of a general degradation of the structural quality of the CIS_2 layers when the temperature of deposition decreases.

C. CIS_2/Mo interface

As already indicated, the Raman spectra measured at depths close to the CIS_2/Mo interface show, in some cases, the presence of additional modes at 382 and 408 cm^{-1}. To clarify the origin of these modes, these spectra were compared with that measured from a sulfurized Mo layer

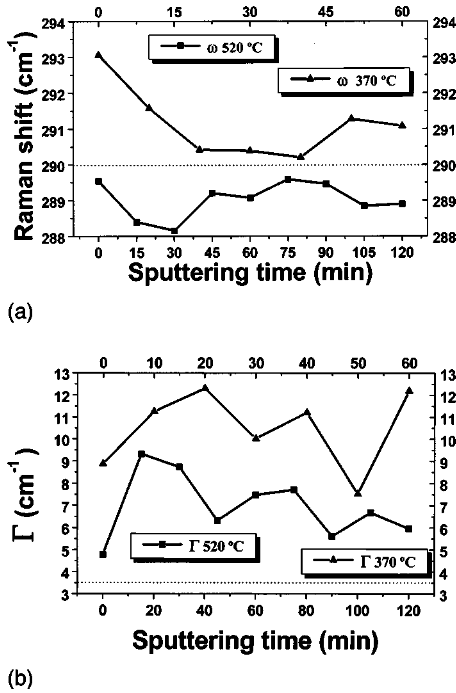

FIG. 6. Position (a) and FWHM (b) of the A_1 Raman peak vs sputtering time from the sputtered Cu-rich etched samples deposited at 520 and 370 °C. Dotted lines indicate the spectral features of the A_1 mode as measured from the reference sample.

(MoS_2). Figure 7 shows the spectra measured from the MoS_2 layer, together with those from the interface region of the Cu-rich and Cu-poor samples deposited at high temperature. As shown in Fig. 7, the spectrum from the MoS_2 layer is characterized by two intense modes at the same position. This clearly indicates the formation of a MoS_2 secondary phase at this interface. This has also been corroborated by XRD measurements, which show peaks characteristic from this phase. In both cases (Cu poor, Cu rich), decreasing the temperature of deposition leads to the disappearance of these modes, which suggests that formation of the MoS_2 phase is

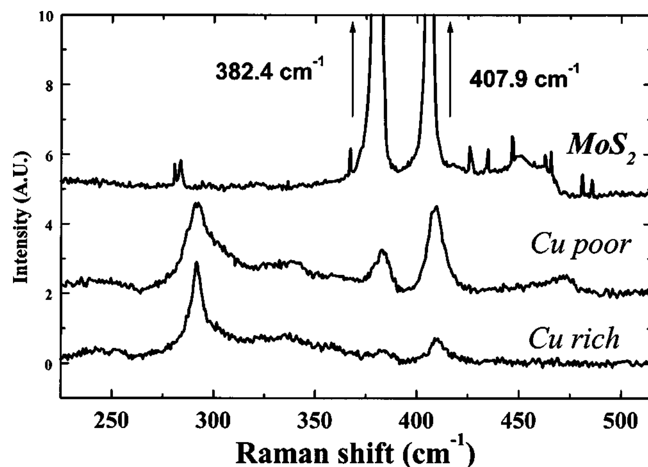

FIG. 7. Raman spectra measured at the CIS_2/Mo interface from the Cu-rich and Cu-poor samples deposited at 520 °C, together with the spectrum from a reference MoS_2 layer.

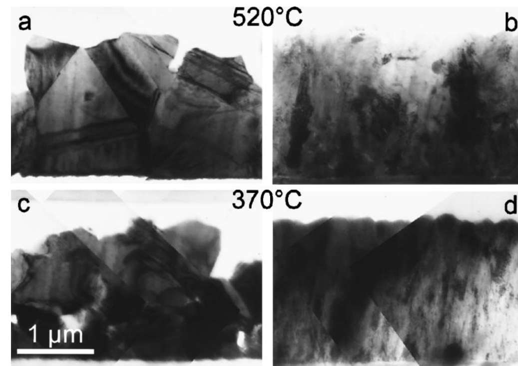

FIG. 8. TEM cross-section images of the samples deposited at 520 °C (a) Cu rich and (b) Cu poor and at 370 °C (c) Cu rich and (d) Cu poor.

also inhibited at low temperature. Also, the intensity of MoS_2 modes from the Cu-poor sample is higher than that from the Cu-rich one.

The presence of a MoS_2 interficial phase in polycrystalline CIS_2 layers on Mo has already been reported by Scheer and Lewerenz.[7] This is similar to $CuInSe_2$/Mo structures, where a $MoSe_2$ phase has been observed by high-resolution TEM.[8] $MoSe_2$ formation has been observed mainly in (In,Ga)-rich layers from $Cu(InGa)Se_2$ solar cells, and it is not as clear in Cu-rich layers. This also agrees with the behavior reported in Fig. 7 and can be interpreted as being due to a low reactivity between the Mo film and the Cu-rich layers. These compounds are characterized by having a layered structure, where bonding between adjacent layers is done by van der Walls forces. This could lead to a decrease in the adherence of the CIS_2 layers to the Mo backcontact in the solar cell device. Poor CIS_2 adherence to the backcontact constitutes one of the main problems of CIS_2-based solar cells. However, the role of MoS_2 in this case is not clear, adherence problems occur mainly for Cu-rich layers obtained following a sequential sputtering deposition process,[1,9] when Cu excess tends to inhibit the formation of this secondary phase.

D. Transmission electron microscopy

Figure 8 shows the cross-section images of the Cu-rich and Cu-poor samples deposited at 520 and 370 °C. The comparison between the four images clearly shows the structural differences from the Cu-poor and Cu-rich sides, as well as the influence of the deposition temperature: Cu-rich layers present a much larger grain size and roughness, whereas Cu-poor areas show a smaller grain size, with a very smooth surface and a very high density of planar defects inside the grain.

The grain size in the Cu-rich side of the samples ranges from about 0.8 ± 0.2 μm for the sample deposited at the lowest temperature of 370 °C up to about 1.6 ± 0.5 μm for the highest temperature, as can be seen in Figs. 8(a) and 8(c). This behavior agrees with the structural degradation already suggested by both the spectral features of the A_1 CIS_2 mode

and the appearance of the 305 cm^{-1} mode at low temperature of deposition. Furthermore, the roughness of these samples is of the order of the grain size.

For the Cu-poor areas, the grains present a rather columnar shape, but their size is difficult to determine due to the extremely high density of defects which are at their inside. From Figs. 8(b) and 8(d), which correspond to the Cu-poor areas of both samples deposited at the highest and lowest temperatures, respectively, one would say that the grain size is slightly larger for the higher temperature. This can be seen in the images, where some grains, which are almost perfectly oriented along low-index zone axis, appear dark in the images. The size of one of these dark zones is larger for the higher temperature. Consistent with this result is the roughness, which is larger (about 150 nm) for the higher temperature sample. These results are further confirmed by electron diffraction patterns, which are characterized by the presence of streaks, a clear indication of the existence of high densities of planar defects inside the grains, well aligned along determined crystallographic directions. In principle, these planar defects can contribute to the observed broadening of the A_1 Raman mode from Cu-poor samples, due to the decrease of the phonon lifetime induced by the defects. Defects can also induce a shift of the mode, due to phonon confinement effects. However, for this the average distance between defects which break the translational symmetry of the crystal and confine the phonons has to be of the order of few nm. Then, the observed blueshift of the A_1 mode from Cu-poor samples is more likely related to residual stress in the Cu-poor CIS_2 lattice.

On the other hand, in these samples it has been impossible to identify the presence of the $CuIn_5S_8$ additional phase observed by Raman scattering, probably a consequence of the small grain size. At the CIS_2/Mo interface region, the presence of the MoS_2 phase has not been detected, which is probably due to its reduced thickness. Furthermore, energy dispersive x-ray measurements cannot help in this case, as the S_K peak overlaps the Mo_L one.

Previous observation of polycrystalline layers deposited by both coevaporation and sequential sputtering processes under Cu-excess conditions has revealed additional spots in the electron diffraction pattern that correspond to CuAu order. The coexistence of both chalcopyrite and CuAu ordering has been observed in epitaxial $CuInS_2$ films by Su and Wei.[10] This has been interpreted as related to the small difference in the energy of formation of both phases, which is 2 meV/atom, according to their calculation. The presence of CuAu ordering from Cu poor samples is not clear in this experiment, and has still to be clarified.

IV. DISCUSSION

The high Cu content in the Cu-rich layer grown at low temperature gives indirect evidence on the inhibition in the segregation of excess Cu at the surface of the layer in the form of CuS. Segregation of Cu excess at the surface in the form of CuS or Cu_2S allows the formation of stoichiometric CIS_2 layers with improved crystallinity (higher grain sizes and lower defect densities).[7] The inhibition in the formation of the CuS secondary phase at the surface of the film for low-temperature deposition conditions could be related to a strong decrease in the mobility of cation (Cu,In) atoms during growth of the films. Excess Cu atoms in the CIS_2 grains cannot diffuse toward grain boundaries, avoiding Cu segregation at the surface. However, accommodation of such a high Cu content in the CIS_2 grains is not clear, and the presence of a Cu-rich secondary phase in the layer cannot be excluded, although no experimental evidence has been obtained from Raman scattering and XRD measurements.

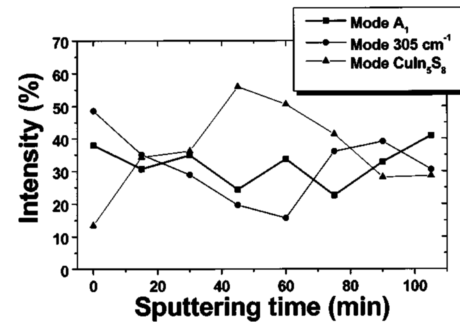

FIG. 9. Relative intensity of the mode A_1, the mode at 305 cm^{-1}, and the $CuIn_5S_8$ modes in the Raman spectra vs sputtering time from the Cu-poor sample deposited at 520 °C [the spectra are plotted in Fig. 2(a)].

Decreasing the temperature of deposition also leads to a significant inhibition in the observation of other secondary phases in the Raman spectra, such as MoS_2 at the interface region from both Cu-rich and Cu-poor layers and $CuIn_5S_8$ from Cu-poor layers. This is also accompanied by the presence of the 305 cm^{-1} mode in the Raman spectra, which correlates with an increase in both blueshift and broadening of the A_1 Raman line. The comparison between the Raman spectra and the AES data shows that the additional 305 cm^{-1} mode is not directly related to the In content. All this gives support to a structural-related origin of the mode.

However, the correlation between the intensity of the A_1 mode and the spectral features of the A_1 peak does not stand for the central region of the Cu-poor sample deposited at high temperature, where a significant $CuIn_5S_8$ contribution is found. This can be seen in Fig. 9, where the relative intensity of the A_1 CIS_2 mode, the additional 305 cm^{-1} mode, and the $CuIn_5S_8$ modes are plotted versus sputter time. In this case, the relative intensity of the 305 cm^{-1} additional mode decreases in the region where a maximum contribution of the $CuIn_5S_8$ secondary phase is detected, which also corresponds to the region with maximum blueshift and broadening of the A_1 CIS_2 mode [Figs. 3(a) and 3(b)]. This suggests that the shift and broadening of the A_1 mode in this heterogeneous region with both CIS_2 and $CuIn_5S_8$ phases is due to additional features such as stress.

Similar data have been obtained by Winkler *et al.*[11] from the Raman scattering and structural analysis of Cu–In–S-based layers. In this work, in-depth Raman spectra were measured from samples beveled by ion etching, and the observed blueshift of the A_1 mode in the region where the $CuIn_5S_8$ phase is detected was attributed to built-in internal

stress. The origin of this internal stress has still to be clarified. As already indicated, XRD shows the existence of a random orientation of $CuIn_5S_8$ crystals. For $CuInS_2$, the XRD spectra show a higher intensity of (112) peaks, which indicates a partial preferential orientation of the $CuInS_2$ crystals from Cu-rich sample growth at high temperature. This suggests the absence of a coherent relationship between both phases, which are more likely separated by well-defined grain boundaries without any preferential relative orientation of both CIS_2 and $CuIn_5S_8$ crystals. According to Winkler *et al.*,[11] compressive stress in the CIS_2 grains could originate at the $CIS_2/CuIn_5S_8$ interfaces, related to different thermal properties of both materials during cool-down of the film. This would also be accompanied by a corresponding tensile stress in the $CuIn_5S_8$ phase. From Fig. 3(a), a stress-induced shift in the layers is in the range of 2.5 cm^{-1}, which corresponds to an average compressive stress level of about 0.5 GPa. Then, the decrease in the intensity of the 305 cm^{-1} mode could be related to an enhancement of lattice ordering in the CIS_2 phase, likely being the excess of cations in this region accommodated in the $CuIn_5S_8$ phase.

In relation to the additional mode in the Raman spectra at 305 cm^{-1}, this could be related to changes in the arrangement of Cu and In atoms in the cation sublattice. In principle, $CuInS_2$ can be arranged in three different crystalline phases, chalcopyrite being the most stable phase at 0 K. At high temperatures (above 1200 K), the most thermodynamically stable phase is sphalerite, where Cu and In atoms are randomly distributed in the tetragonal cation sublattice.[12] At intermediate temperatures, the CuAu cationic ordering becomes metastable.

To clarify the possible correlation of the 305 cm^{-1} mode with the sphalerite phase, XRD measurements have been carried out in the samples. The distinction between the chalcopyrite and the sphalerite (zinc-blende-like) structures by XRD is compromised by the similarity of the spectra. In principle, there are two main differences between them. First, reflections allowed for the chalcopyrite structure corresponding to (hkl) planes with k even and (hl) odd, or with h even and (kl) odd, are not allowed for the zinc-blende structure. The most intense reflections are the following:

(hkl)	2θ (λ=1.5418 Å)
(101)	17.9
(103)	29.0
(211)	37.3
(213)	44.1

The other characteristic difference is the splitting of some of the peaks associated with equivalent planes in the sphalerite structure, which correspond to different atomic planes in the chalcopyrite structure. The most intense splittings are

$$(200)_{\text{sphalerite}} \Rightarrow [(004)+(200)]_{\text{chalcopyrite}}, \quad \text{at } 32.2°/32.4°,$$

$$(220)_{\text{sphalerite}} \Rightarrow [(220)+(204)]_{\text{chalcopyrite}}, \quad \text{at } 46.4°/46.5°,$$

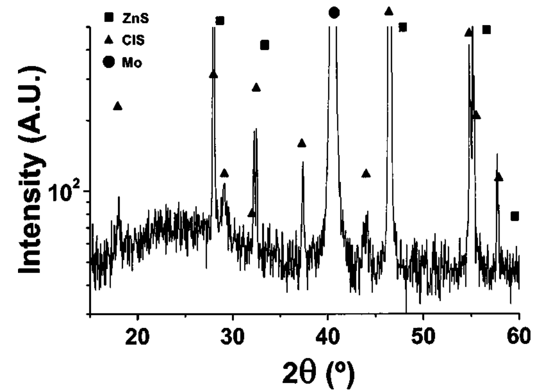

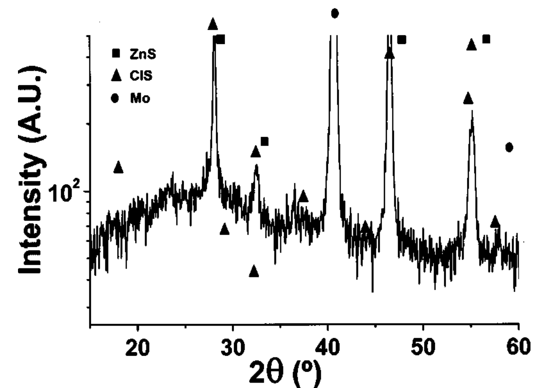

FIG. 10. XRD spectra from Cu poor etched samples deposited at (a) 520 and (b) 370 °C. The position of peaks corresponding to sphalerite (zinc blende), chalcopyrite (CIS_2), and Mo structures are indicated in the spectra.

$$(311)_{\text{sphalerite}} \Rightarrow [(312)+(116)]_{\text{chalcopyrite}}, \quad \text{at } 54.8°/55.1°.$$

Figures 10(a) and 10(b) show the XRD spectra from the Cu-poor samples deposited at high temperature and low temperature, respectively. The first spectrum is characterized by the presence of the different peaks related to the chalcopyrite phase, and in principle, no evidence of the sphalerite phase is given. In the second case, all reflections forbidden for the sphalerite structure are absent in the spectrum, and splitting of the modes characteristic of the chalcopyrite phase does not seem to occur. This suggests the presence of the sphalerite phase at the Cu-poor region from the layer deposited at low temperature. However, the differences between both spectra could also be related to the poorer structural quality of the CIS_2 layer growth at low temperature, due to the decrease in the intensity of the XRD peaks and the increase in their FWHM. In any case, the absence of any evidence related to the sphalerite phase in the Cu-poor sample deposited at high temperature does not support the assignment of the 305 cm^{-1} mode in the Raman spectra with this phase. This agrees with recent results on Raman polarization measurements performed in epitaxial $CuInS_2$ layers, which show both the CIS_2 A_1 mode and the additional 305 cm^{-1} mode to be totally symmetric.[13] This suggests this mode to be related to CuAu ordering or to local arrangements of atoms giving rise to a local vibrational mode. The presence of

CuAu ordering in the polycrystalline layers is still not clear, and further measurements are in progress to clarify this issue.

Finally, we have to remark that coevaporation has been chosen as a preparation method for this work because of the possibility to grow samples with a lateral gradient in composition. We note that Raman spectra as well as cell characteristics are quite similar when a sequential preparation process[9] is used. The best cells have an active area efficiency in the range of 12%–13%.[14,15] There is a clear correlation between the results presented here and the cell performance: Cu-poor films, due to their high defect density even if grown at high substrate temperatures, are heavily compensated and semi-insulating. Without additional efforts (doping, flux assisted growth[16]), only films grown under Cu excess are suitable for solar cells. In the latter case, the minimum substrate temperature that yields good devices is on the order of 500 °C, i.e., in the same temperature range where we found complete segregation of the Cu excess to the surface and where the 305 cm^{-1} additional mode disappears from the Raman spectrum. Significantly higher substrate temperatures are not considered because they would not be compatible with the soda lime glass substrates.

V. CONCLUSIONS

The detailed microstructural characterization of $CuInS_2$ polycrystalline films by combining in depth micro-Raman scattering and Auger electron spectroscopy measurements as a function of the chemical composition and temperature of processing has allowed us to identify the main secondary phases in the layers as $CuIn_5S_8$ for Cu-poor samples and CuS for Cu-rich ones. $CuIn_5S_8$ mainly appears at the central region of the layers, whereas CuS segregates at the surface. Moreover, in both cases a MoS_2 secondary phase is also observed at the CIS_2/Mo interface region, although the comparison between the Raman spectra suggests a lower occurrence of this phase for Cu-rich layers.

The presence of these secondary phases is strongly related to the temperature of processing: these secondary phases are inhibited when the growth temperature decreases to 420 °C. This is also accompanied by a significant degradation of the structural CIS_2 features, as reflected by the increase in both shift and broadening of the A_1 CIS_2 mode in the spectra, and by the decrease of the grain size estimated by cross-section TEM. Also, Raman spectra measured from samples grown at lower temperatures are characterized by the presence of an additional mode at about 305 cm^{-1}, which gives additional support to its previously proposed structural origin. The complementary analysis of the layers by TEM and XRD suggests that the sphalerite structure is not directly related to this additional mode, which could be more likely related to either CuAu ordering or to local arrangements of cations (maybe rich in In atoms) vibrating around S anions.

ACKNOWLEDGMENTS

This work has been partially funded by the Joule III Program of the European Commission (Contract No. JOR3-CT98-0297). O. Van der Biest, from the Katholieke Universiteit Leuven, is acknowledged for allowing access to the TEM of his department.

[1] K. Siemer, J. Klaer, I. Luck, J. Bruns, R. Klenk and D. Bräunig, Sol. Energy Mater. Sol. Cells (to be published).
[2] T. Jawhari and A. Pérez-Rodríguez, The Internet Journal of Vibrational Spectroscopy **2**, 6/41 (1999).
[3] J. Álvarez-García, J. Marcos-Ruzafa, A. Pérez-Rodríguez, A. Romano-Rodríguez, J. R. Morante, and R. Scheer, Thin Solid Films **361/362**, 208 (2000).
[4] A. Pérez-Rodríguez, J. Álvarez-García, J. Marcos-Ruzafa, A. Romano-Rodríguez, J. R. Morante, R. Scheer, J. Klaer, and R. Klenk, *Fourth International Conference on Optical Diagnostics of Materials and Devices for Opto-, Micro- and Quantum Electronics* (Kiev, Ukraine, 1999); Proc. SPIE (to be published).
[5] J. Marcos-Ruzafa, A. Romano-Rodríguez, J. Álvarez-García, A. Pérez-Rodríguez, J. R. Morante, J. Klaer, and R. Scheer, Inst. Phys. Conf. Ser. **164**, 247 (1999).
[6] N. M. Gasanly, S. A. El-Hamid, L. G. Gasanova, and A. Z. Magomedov, Phys. Status Solidi B **169**, K115 (1992).
[7] R. Scheer and H.-J. Lewerenz, J. Vac. Sci. Technol. A **13**, 1924 (1995).
[8] T. Wada, Inst. Phys. Conf. Ser. **152**, 903 (1998).
[9] J. Klaer, J. Bruns, R. Henninger, K. Siemer, R. Klenk, K. Ellmer, and D. Bräunig, Semicond. Sci. Technol. **13**, 1456 (1998).
[10] D. S. Su and S.-H. Wei, Appl. Phys. Lett. **74**, 2483 (1999).
[11] M. Winkler, O. Tober, J. Penndorf, K. Szulzewsky, D. Röser, G. Lippold, and K. Otte, Thin Solid Films **361-362**, 273 (2000).
[12] S.-H. Wei, L. G. Ferreira, and A. Zunger, Phys. Rev. B **45**, 2533 (1992).
[13] J. Alvarez-García, A. Pérez-Rodríguez, A. Romano-Rodríguez, T. Jawhari, J. R. Morante, R. Scheer, and W. Calvet, Thin Solid Films (to be published).
[14] D. Braunger, Th. Dürr, D. Hariskos, Ch. Köble, Th. Walter, N. Wieser, and H. W. Schock, Proceedings of the 25th IEEE Photovoltaic Specialists Conference, 1996 p. 1001.
[15] K. Siemer, J. Klaer, I. Luck, J. Bruns, R. Klenk, and D. Bräunig, Solar Energy Mater. Sol. Cells (in press).
[16] T. Watanabe and M. Matsui, Jpn. J. Appl. Phys., Part 2 **38**, L1379 (1999).